

Numerical investigation of the performance of AlGa_N/Ga_N/BGa_N double-gate double-channel high electron mobility transistor

Hamida Djelti

Department of Telecommunications, System and Technology of Information and Communication Laboratory, Abou-bekr Belkaid University of Tlemcen, Chetouane, Algeria

Article Info

Article history:

Received Jan 17, 2021

Revised Jan 27, 2022

Accepted Feb 6, 2022

Keywords:

AlGa_N/Ga_N

BGa_N

Double-channel

Double-gate

HEMT

ABSTRACT

In this work, we examine the direct-current (DC) behavior and the radio frequency (RF) performance of both single-gate simple-channel (SGSC), single-gate double-channel (SGDC) and double-gate double-channel (DGDC) AlGa_N/Ga_N/BGa_N high electron mobility transistor (HEMT) with BGa_N back-barriers consist of 250 nm gate length. Using technology computer aided design (TCAD) Silvaco, our isothermal simulation results reveal that the proposed structure of double-gate double-channel HEMT with BGa_N back-barriers (DGDCBB HEMT) increases electron concentration and consequently the saturation drain current, breakdown voltage, the transconductance. On the other hand, decreases the gate leakage current compared to a conventional HEMT and to a double-channel HEMT back-barriers. Furthermore, the proposed double-gate double-channel back-barrier HEMT device shows good cutoff frequency (94 GHz) and a maximum oscillation frequency (170 GHz). These results suggest that double-gate double channel HEMT back-barriers could be useful for high frequency and high-power microwave applications.

This is an open access article under the [CC BY-SA](#) license.



Corresponding Author:

Hamida Djelti

Department of Telecommunications, STIC Laboratory, Abou-bekr Belkaid University of Tlemcen Chetouane, Algeria

Email: djelti_hamida@yahoo.fr

1. INTRODUCTION

Recently, III-N Nitride semiconductor materials such as gallium nitride (Ga_N) and its alloys has an excellent physical, electrical and thermal properties, these properties include in particular the excellent wide band gap energy (3.43 eV), high saturation velocity (3×10^7 cm/s), high thermal conductivity (1.3 W/cmK) [1], [2], high optical phonon energy (87.3 meV), and high critical electric field (150 Kv/cm) which are a great reasons for its usage in high temperature, high-speed and for next-generation power applications [3], [4]. New telecommunications systems require very fast and low noise circuits. Compared to silicon (Si), the physical properties of III-N materials (such as AlGa_N, InGa_N, BGa_N and Ga_N) are the most suitable for this type of radio-frequency (RF) application. The most commonly used field effect transistor to design these systems is the high-electron mobility transistors (HEMTs).

The HEMT technology based on aluminium gallium nitride (AlGa_N)/gallium nitride (Ga_N) hetero interface are appealing for power-switching, high temperature and millimeter-wave applications because this device has an excellent electronic properties, such as high breakdown field, high mobility and high sheet-carrier density of the two-dimensional electron gas (2-DEG [5], [6] comparing with conventional HEMTs devices [7], [8]. Despite the interesting characteristics of the HEMTs transistors, there are many parasitic

effects which severely limits the direct-current characteristics and the radio-frequency performance of AlGa_xN/GaN-based HEMTs, such effects include current collapse, gate and drain lag, self-heating effects, the trapping effects. These undesirable effects have been analyzed and reported by several researchers [9]–[18]. As well known, from a physical point of view, the origin of the trapping effects on AlGa_xN/GaN HEMT is associated with the presence of traps positioned in the GaN buffer layer or at the device surface [14].

In the previous work, the degradation of the trapping effect in the AlGa_xN/GaN HEMT have been realized by including the boron (B) into gallium nitride (GaN) binary, because boron gallium nitride (BGaN) alloys possess very interesting physical properties [19], [20]. However, it is demonstrated that the leakage current in the GaN buffer layer decreases by the use of BGaN as back-barrier layers, on the other hand, the resistivity of the epitaxial layer of HEMTs devices increases [21]–[23]

In order to improve the performance, and reliability of AlGa_xN/GaN HEMT, we propose in this paper a novel structure double-gate double-channel HEMT wurtzite AlGa_xN/GaN with B_{0.01}Ga_{0.99}N back barrier and compare its direct-current (DC) and RF characteristics with the conventional and double-channel AlGa_xN/GaN/BGaN HEMT. Numerical devices isothermal simulations are performed to describe significant physics in the DC and the alternate current (AC) performance of Al_{0.26}Ga_{0.74}N/GaN/B_{0.01}Ga_{0.99}N HEMTs with gates length of 250 nm by using calibrated TCAD models. Also, we address the relative merits of each technology.

The following section includes the physical model in terms of the basic differential equations and the materials model employed for the analysis of Al_{0.26}Ga_{0.74}N/GaN/B_{0.01}Ga_{0.99}N HEMT. Section 3 shows the devices structures of this work. In section 4, the results of the simulated DC and RF characteristics are discussed and explained in detail, a comparison of our simulation results is made to validate the results and consequently prove the importance of this research on HEMT based GaN and its alloys materials for the high-frequency and high-power circuits and systems applications. Finally, conclusions are presented.

2. PHYSICAL MODEL OF ALGAN/GAN/BGAN HEMT

The direct-current network characteristic of AlGa_xN/GaN/BGaN HEMTs is determined by using the drift-diffusion transport model. Generally, the basic differential equations governing the physical and electrical operation of the HEMT transistor are equations of potential and electron and hole concentrations. The conventional formulation of drift-diffusion equations in terms of the electron and hole current densities are expressed as (1) and (2) [24]:

$$\vec{J}_n = qn \mu_n \vec{E}_n + qD_n \nabla n \quad (1)$$

$$\vec{J}_p = qp \mu_p \vec{E}_p - qD_p \nabla p \quad (2)$$

where, μ_n and μ_p are the electron and hole motilities, D_n and D_p are diffusion coefficients for electron and hole, respectively. The effective electric fields which take account of bandgap narrowing effects are defined as (3), (4) [24]:

$$\vec{E}_n = -\nabla \left(\psi + \frac{kT_L}{q} \ln n_{ie} \right) \quad (3)$$

$$\vec{E}_p = -\nabla \left(\psi + \frac{kT_L}{q} \ln p_{ie} \right) \quad (4)$$

2.1. Materials model

Among the fundamental physical parameters of any semiconductors is the bandgap energy. For Al_xGa_{1-x}N, the variation of the band gap energy with aluminum (Al) composition (x) is expressed as [25]:

$$E_g(x) = (1 - x)E_g(\text{GaN}) + xE_g(\text{AlN}) - bx(1 - x) \quad (5)$$

where, b is the bowing factor ($b \approx 1$ eV), the band gap energy value of GaN, $E_g(\text{GaN}) \approx 3.5$ eV, and the band gap energy value of aluminum nitride (AlN), $E_g(\text{AlN}) \approx 6.1$ eV. For BGaN, the band gap energy of is calculated from [22]:

$$E_g(B_x\text{Ga}_{1-x}\text{N}) = x.E_g(\text{BN}) + (1 - x).E_g(\text{GaN}) - C(1 - x) \quad (6)$$

where, C is the bowing factor ($C = 9.2 \pm 0.5$ eV), the band gap of boron nitride (BN), $E_g(\text{BN}) = 5.5$ eV [26].

The band diagrams of heterojunctions interface aligned by Anderson's electron affinity X model. The variation of the electron affinity directly contributes to the variation of band alignments given as (7) [27].

$$\frac{\Delta E_c}{\Delta E_v} = \frac{0,7}{0,3} \quad (7)$$

For $Al_xGa_{1-x}N$ and $B_xGa_{1-x}N$, the dependence of the dielectric permittivity with the composition fraction (x) of gallium is calculated as (8), (9) [28]:

$$\epsilon(Al_xGa_{1-x}N) = 8.5x + 8.9(1 - x) \quad (8)$$

$$\epsilon(B_xGa_{1-x}N) = 7.1x + 8.9(1 - x) \quad (9)$$

The effective masses for AlGaN and B GaN alloys as a function of composition fraction x of gallium is given as (10) to (13) [29].

$$m_e(Al_xGa_{1-x}N) = 0.314x + 0.2(1 - x) \quad (10)$$

$$m_h(Al_xGa_{1-x}N) = 0.417x + 1.0(1 - x) \quad (11)$$

$$m_e(B_xGa_{1-x}N) = 0.35x + 0.21(1 - x) \quad (12)$$

$$m_h(B_xGa_{1-x}N) = 0.37x + 1.0(1 - x) \quad (13)$$

The dependence of the electric field with mobility is defined by the following Caughey and Thomas expression that takes account the saturation velocities $vsatn$ and $vsatp$ of electrons and holes, respectively [30]:

$$\mu_n(E) = \mu_{n0} \left[\frac{1}{1 + \left(\frac{\mu_{n0}E}{vsatn}\right)^{\beta n}} \right]^{1/\beta n} \quad (14)$$

$$\mu_p(E) = \mu_{p0} \left[\frac{1}{1 + \left(\frac{\mu_{p0}E}{vsatp}\right)^{\beta p}} \right]^{1/\beta p} \quad (15)$$

where, βn and βp are constants, μ_{n0} , μ_{p0} are the electron and hole mobilities at low electric field, and E is the parallel electric field. Using the software package Atlas from Silvaco, we specified drift-diffusion model with Gummel-Newton method and their coefficients for each material such as AlGaN, GaN, B GaN, AlN, ..., also, we specified the bandgap energy, electron affinity, permittivity, conduction and valence band density of states, mobility, velocity, impact ionization effect (local and non-local), with material and mobility statements.

3. PROPOSED DEVICES STRUCTURES

The proposed devices structures which are analyzed and simulated using Atlas of Silvaco TCAD software [31], along with the devices dimensions and material of various layers used is presented in Figure 1 and Figure 2. The conventional structure of simple-gate simple-channel (SGSC) HEMT with B GaN back barriers is reported by Gassoumi *et al.* [32]. In this work, the gate(s) length of the proposed devices structures of both simulated SGDC HEMT and DGDC HEMT with B GaN back barriers is 250 nm, the structures consists of silicon as substrate, an undoped AlN/AlGaN buffer layer with a thickness of 500 nm, followed by a 1800 nm undoped GaN channel, a 23 nm thickness of undoped $Al_{0.26}Ga_{0.74}N$ barrier layer. Finally, 1 nm was added as n+ GaN cap layer. For SGDC HEMT, the gate-source and the gate-drain spacing are 0.77 μm and 1.32 μm , respectively. For DGDC HEMT, the gate-source and the gate-drain spacing are 0.5 μm and 0.84 μm respectively, the gate1 (G1)-to-gate2 (G2) distance is 0.5 μm .

We draw in Figure 3 the energy band diagram in term of the conduction band energy at thermodynamic equilibrium along the vertical direction of the AlGaN/GaN/AlGaN/GaN/B GaN HEMT. From Figure 3, we observed that the band diagram is correct, because the barrier height (marking the border between the Schottky contact and the ca layer) is 1 eV. In addition, the quantum well created by the

conduction band discontinuity at the heterojunctions interface between the channels and the confinement barrier have a sufficient depth for the electrons to occupy its energy levels.

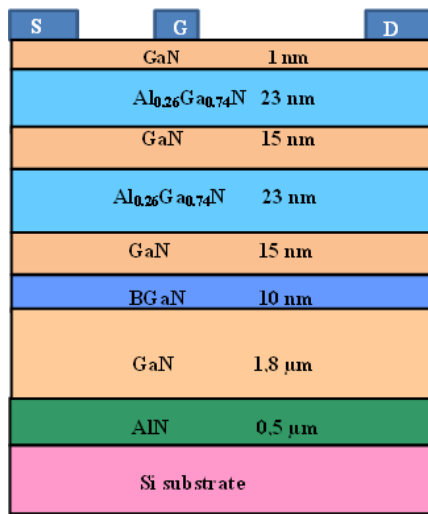


Figure 1. Topology of the proposed SGDC-HEMT with BGaN back-barriers

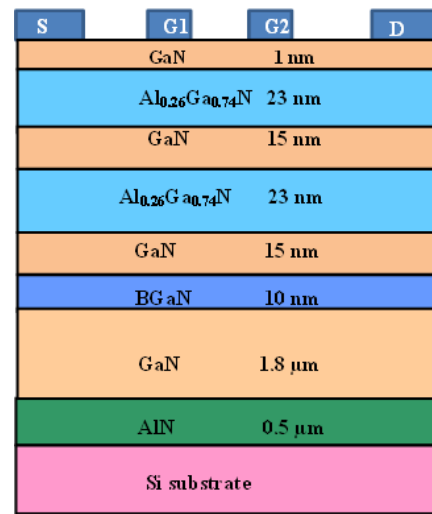


Figure 2. Topology of the proposed DGDC-HEMT with BGaN back-barriers

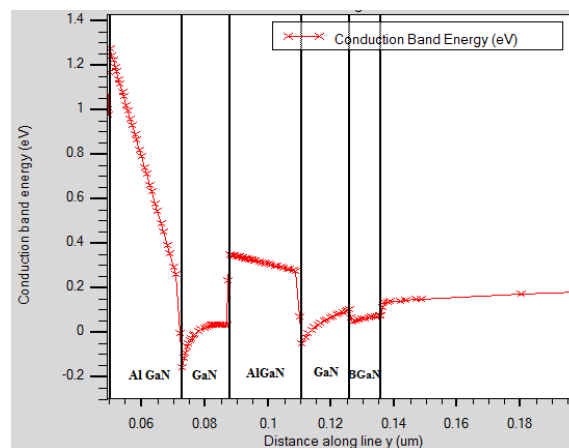


Figure 3. Conduction band of double-gate double-channel AlGaN/GaN/AlGaN/GaN/BGaN HEMT

4. RESULTS AND DISCUSSION

In order to validate our proposed structures, we compare our output characteristic simulation results as shown in Figure 4 with output characteristic simulation results reported by [32] in Figure 5 of single channel HEMT with BGaN back-barriers. Clearly, from Figures 4 and 5 and for all gate-source voltage, we observed a good similarity between our simulations results and the simulation results of [32]. Figures 6 and 7 shows output current-voltage (I - V) characteristics for double-channel HEMT and double-gate double channel HEMT with BGaN back-barriers, respectively. The gate voltage range is from 0.0 to -5.0 V. We observed in Figures 6 and 7 a good pinch-off and saturation current characteristics for two proposed devices. Due to the incorporation of the second channel and BGaN as a confinement barrier in the structures, the double-channel HEMT and double-gate double-channel HEMT operated at higher gate-source and drain-source voltage, which can enhance the current driving capability. From Figures 6 and 7, we can see at $V_{gs}=0.0$ V, the maximum saturation drain current for simple-gate double-channel HEMT and double-gate double-channel HEMT were 0.7 A and 0.6 A, respectively. These values of the maximum saturation drain current indicate that our obtained results are one of the highest reported values compared to [33], [34] and proves the efficacy of the proposed designs.

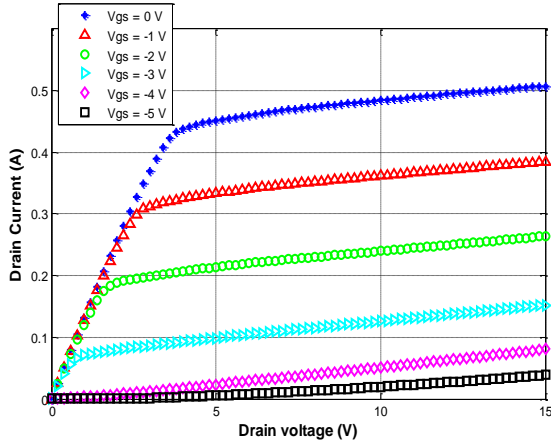


Figure 4. Our simulated output characteristics of AlGaIn/GaN/BGaIn HEMT

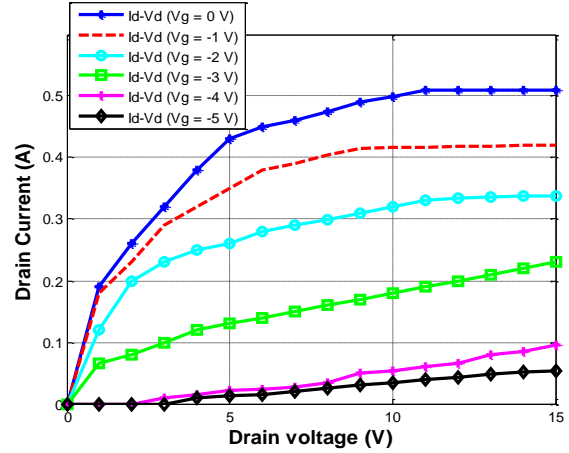


Figure 5. Simulated output characteristics of AlGaIn/GaN/BGaIn HEMT [32]

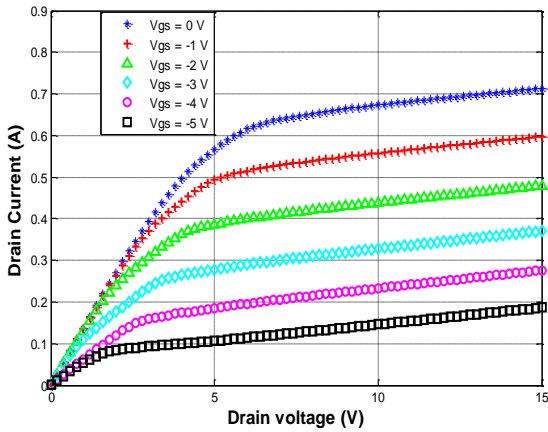


Figure 6. Simulated output characteristics of simple-gate double-channel HEMT with BGaN back-barriers

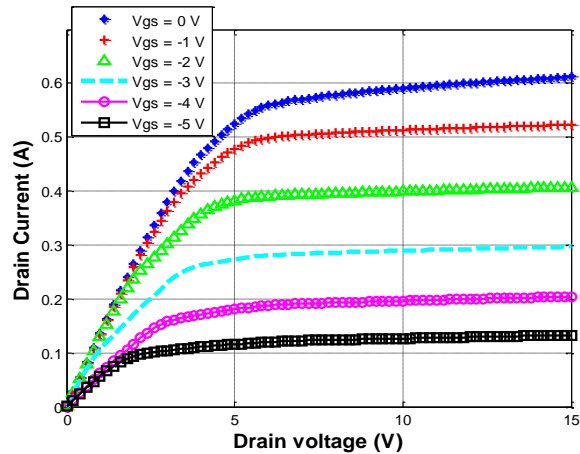


Figure 7. Simulated output characteristics of double-gate double-channel HEMT with BGaN back-barriers

Figure 8 depicts the transfer characteristics for three heterostructures: simple-gate simple-channel (SGSC), simple-gate double-channel (SGDC) and double-gate double-channel (DGDC) HEMT with BGaN back-barriers, the drain voltage fixed at 15 V, and the gate voltage range is from 1.0 to -10.0 V. As shown in Figure 8, we note that the threshold voltage (V_{th}) decreases from -4.27 V (threshold voltage of SGSCBB HEMT) to -5.91 V (threshold voltage of SGDCBB HEMT), which makes it possible to increase the carrier density of the two-dimensional electron gas (2-DEG), and consequently leads to an increase in the performance of devices in term of power. Also, we note that the device double-gate double-channel HEMT with back-barriers (DGDCBB HEMT) presents a Very small threshold voltage shift is equal to -4.95 V which due to an excellent control of the channel.

Figure 9 illustrate the gate-source current versus the gate-source voltage of simple-gate simple-channel back-barriers HEMT (SGSCBB HEMT), simple-gate double-channel back-barriers HEMT (SGDCBB HEMT) and double-gate double-channel back-barriers HEMT (DGDCBB HEMT) at $V_{ds}=15$ V. From Figure 9, we can see that very low gate leakage current is observed in these devices confirming an electron injection into the buffer layer (AlGaIn) and suppressing a surface leakage problem for the AlGaIn/GaN HEMT with BGaN back-barriers structure. In particular, in the double-gate double-channel HEMT with BGaN back barriers exhibit favorable device performance in term of reduction and alleviated of the current collapse.

Figure 10 presents the variation of the transconductance (G_m) as a function of gate-source voltage of simple-gate simple-channel back-barriers HEMT (SGSCBB HEMT), simple-gate double-channel back-

barriers HEMT (SGDCBB HEMT) and double-gate-double-channel back-barriers HEMT (DGDCBB HEMT), the bias applied to the drain is 15 V. The simulated double-gate double-channel HEMT with BGaN back barriers exhibit a maximum transconductance of 124 mS/mm at 0.0 V gate-source voltage.

To investigate high frequency characteristics of the devices, S-parameters were simulated with Atlas from Silvaco software. Figures 11 and 12 depicts the variation of the current gain (H21) and unilateral power gain versus frequency on a logarithmic scale at the room temperature, the bias applied to the drain is 15 V, for DGDCBB HEMT, the polarizations applied to the first gate (G1) and the second gate (G2) are 0.0 V and 4 V, respectively. For SGSCBB HEMT and SGDCBB HEMT, the bias applied to the gate is 0.0 V. From Figure 11, the cutoff frequency value for simple-gate simple-channel back-barriers HEMT (SGSCBB HEMT), simple-gate double-channel back-barriers HEMT (SGDCBB HEMT) and double-gate-double-channel back-barriers HEMT (DGDCBB HEMT) is, respectively, 124 GHz, 110 GHz and 94 GHz. From Figure 12, a maximum oscillation frequency for simple-gate simple-channel back-barriers HEMT (SGSCBB HEMT), simple-gate double-channel back-barriers HEMT (SGDCBB HEMT) and double-gate-double-channel back-barriers HEMT (DGDCBB HEMT) is, respectively, 92 GHz, 115 GHz and 170 GHz. These values of cutoff frequency and maximum oscillation frequency indicate that our obtained results are one of the highest reported values compared to the value reached in state of art for similar devices [33], [34].

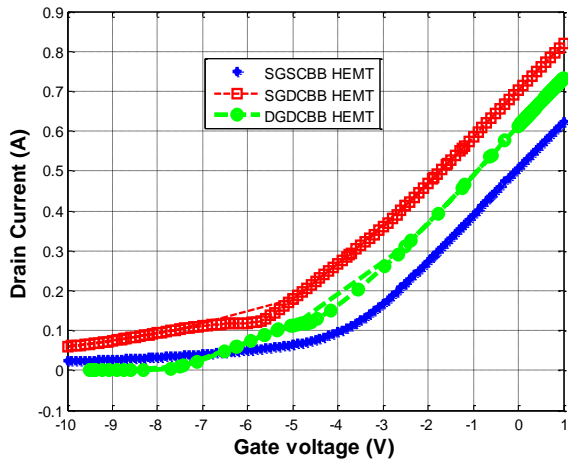


Figure 8. Transfer characteristics of SGSCBB HEMT, SGDCBB HEMT and DGDCBB HEMT at $V_{ds} = 15 V$

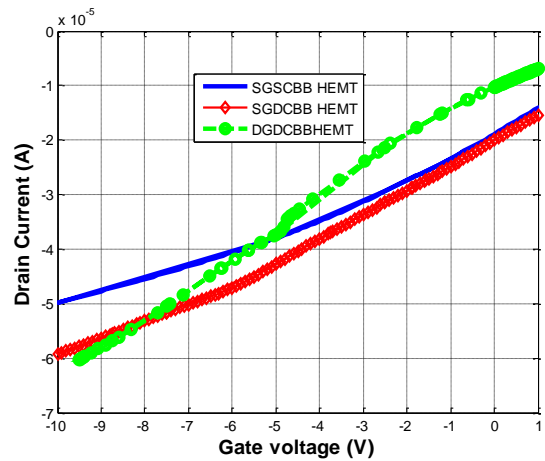


Figure 9. Gate-source current variation of the gate-source voltage in SGSCBB HEMT, SGDCBB HEMT and DGDCBB HEMT at $V_{ds} = 15 V$

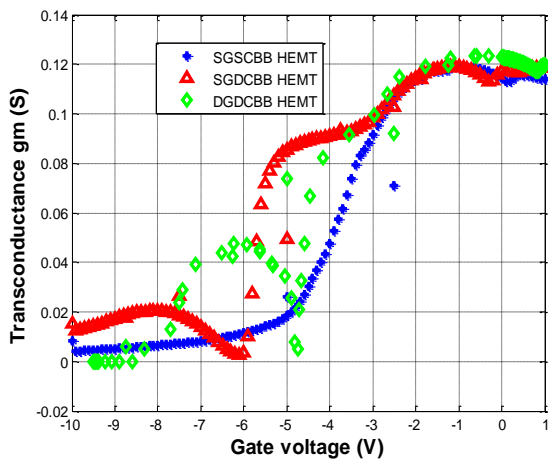


Figure 10. Transconductance versus the gate-source voltage of SGSCBB HEMT, SGDCBB HEMT and DGDCBB HEMT at $V_{ds} = 15 V$

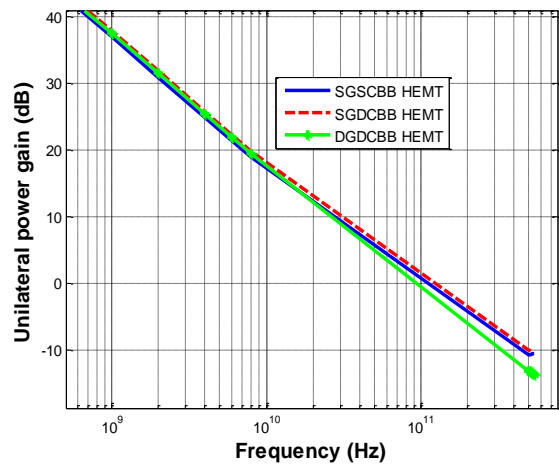


Figure 11. Current gain (H21) of SGSCBB HEMT, SGDCBB HEMT and DGDCBB HEMT at $V_{ds} = 15 V$

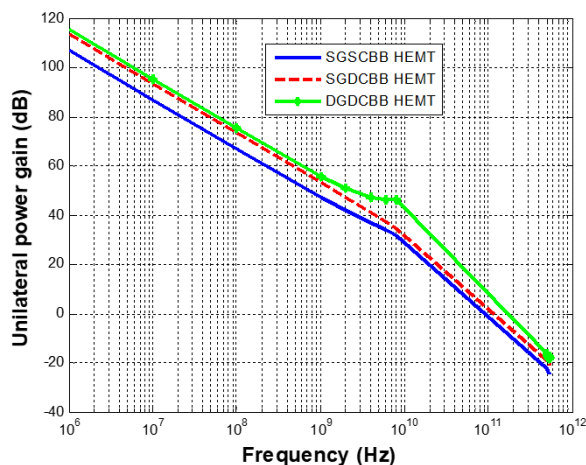


Figure 12. Unilateral power gain (UT) of SGSCBB HEMT, SGDCBB HEMT and DGDCBB HEMT at $V_{ds} = 15$ V

5. CONCLUSION

In conclusion, we presented the isothermal results of the DC and RF performances of the simple-gate simple-channel back-barriers HEMT (SGSCBB HEMT), simple-gate double-channel back-barriers HEMT (SGDCBB HEMT) and double-gate double-channel back-barriers HEMT (DGDCBB HEMT) taking into account the technological parameters in our simulations by using two dimensional device simulator Atlas of TCAD Silvaco. In comparison to SGSCBB HEMT the proposed devices double-gate double-channel back-barriers HEMT (DGDCBB HEMT) with a gate length of 250 nm exhibits a maximum drain current of 0.7 A/mm and 0.6 A/mm, a threshold voltage of -5.91 V and -4.95 V, respectively, a maximum transconductance of 124 mS mm⁻¹ for DGDCBB HEMT, also a very low gate leakage current is observed in our proposed devices. Furthermore, a cutoff frequency of 94 GHz and a maximum frequency of oscillation 170 GHz were achieved which are better than similar technological parameters devices. The both double-channel double-gate and simple-gate double-channel back-barrier devices exhibits favorable devices performance in term of reduction and alleviated of the current collapse. All these excellent performance improvement suggest that our novel double-gate double-channel HEMT with B_{GaN} back is a good candidate which offer attractive results for high power and high frequencies applications.

REFERENCES

- [1] J. A. del Alamo and J. Joh, "GaN HEMT reliability," *Microelectronics Reliability*, vol. 49, no. 9–11, pp. 1200–1206, Sep. 2009, doi: 10.1016/j.microrel.2009.07.003.
- [2] L. Zhu and H. Luo, "On the role of piezoelectricity in phonon properties and thermal conductivity of GaN nanofilms," *Theoretical and Applied Mechanics Letters*, vol. 6, no. 6, pp. 277–281, Nov. 2016, doi: 10.1016/j.taml.2016.11.001.
- [3] Ahmed M. Nahhas, "Review of AlGa_N/Ga_N HEMTs based devices," *American Journal of Nanomaterials*, vol. 7, no. 1, p. 10–21, 2019.
- [4] Y. C. Lin *et al.*, "Gallium nitride (GaN) high-electron-mobility transistors with thick copper metallization featuring a power density of 8.2 W/mm for Ka-band applications," *Micromachines*, vol. 11, no. 2, Feb. 2020, doi: 10.3390/mi11020222.
- [5] Y. Wu, M. Jacob-Mitos, M. L. Moore, and S. Heikman, "A 97.8% efficient GaN HEMT boost converter with 300-W output power at 1 MHz," *IEEE Electron Device Letters*, vol. 29, no. 8, pp. 824–826, Aug. 2008, doi: 10.1109/LED.2008.2000921.
- [6] C.-H. Lee, W.-R. Lin, Y.-H. Lee, and J.-J. Huang, "Characterizations of enhancement-mode double Heterostructure GaN HEMTs with gate field plates," *IEEE Transactions on Electron Devices*, vol. 65, no. 2, pp. 488–492, Feb. 2018, doi: 10.1109/TED.2017.2786479.
- [7] G. Greco, F. Iucolano, and F. Roccaforte, "Review of technology for normally-off HEMTs with p-GaN gate," *Materials Science in Semiconductor Processing*, vol. 78, pp. 96–106, May 2018, doi: 10.1016/j.mssp.2017.09.027.
- [8] K. Mazumdar, S. Kala, and A. Ghosal, "Nanocrack formation due to inverse piezoelectric effect in AlGa_N/Ga_N HEMT," *Superlattices and Microstructures*, vol. 125, pp. 120–124, Jan. 2019, doi: 10.1016/j.spmi.2018.04.038.
- [9] J. M. Tirado, J. L. Sanchez-Rojas, and J. I. Izpura, "Trapping effects in the transient response of AlGa_N/Ga_N HEMT devices," *IEEE Transactions on Electron Devices*, vol. 54, no. 3, pp. 410–417, Mar. 2007, doi: 10.1109/TED.2006.890592.
- [10] H. Mosbahi *et al.*, "Direct-current and radio-frequency characteristics of passivated AlGa_N/Ga_N/Si high electron mobility transistors," *Current Applied Physics*, vol. 13, no. 7, pp. 1359–1364, Sep. 2013, doi: 10.1016/j.cap.2013.04.003.
- [11] F. Jabli, M. A. Zaidi, N. Ben Hamadi, S. Althoyaib, and M. Gassoumi, "Characterisation of the effect of surface passivation with SiO₂/Si₃N₄ on deep levels in AlGa_N/Ga_N/Si HEMTs," *Journal of Alloys and Compounds*, vol. 653, pp. 624–628, Dec. 2015, doi: 10.1016/j.jallcom.2015.09.007.
- [12] M. A. Khan, J. N. Kuznia, M. S. Shur, and Q. C. Chen, "Current/voltage characteristic collapse in AlGa_N/Ga_N heterostructure insulated gate field effect transistors at high drain bias," *Electronics Letters*, vol. 30, no. 25, pp. 2175–2176, Dec. 1994, doi: 10.1049/el:19941461.

- [13] K. Doverspike, S. C. Binari, and W. Kruppa, "Low-frequency dispersion characteristics of GaN HFETs," *Electronics Letters*, vol. 31, no. 22, pp. 1951–1952, Oct. 1995, doi: 10.1049/el:19951298.
- [14] S. C. Binari *et al.*, "Trapping effects and microwave power performance in AlGaIn/GaN HEMTs," *IEEE Transactions on Electron Devices*, vol. 48, no. 3, pp. 465–471, Mar. 2001, doi: 10.1109/16.906437.
- [15] T. Mizutani, Y. Ohno, M. Akita, S. Kishimoto, and K. Maezawa, "A study on current collapse in AlGaIn/GaN HEMTs induced by bias stress," *IEEE Transactions on Electron Devices*, vol. 50, no. 10, pp. 2015–2020, Oct. 2003, doi: 10.1109/TED.2003.816549.
- [16] J. I. Izpura, "Drain current collapse in GaN metal semiconductor field-effect transistors due to surface band-bending effects," *Semiconductor Science and Technology*, vol. 17, no. 12, pp. 1293–1301, Dec. 2002, doi: 10.1088/0268-1242/17/12/315.
- [17] J. Joh, J. A. del Alamo, and J. Jimenez, "A simple current collapse measurement technique for GaN High-electron mobility transistors," *IEEE Electron Device Letters*, vol. 29, no. 7, pp. 665–667, Jul. 2008, doi: 10.1109/LED.2008.2000919.
- [18] O. Mitrofanov and M. Manfra, "Poole-frenkel electron emission from the traps in AlGaIn/GaN transistors," *Journal of Applied Physics*, vol. 95, no. 11, pp. 6414–6419, Jun. 2004, doi: 10.1063/1.1719264.
- [19] S. Gautier *et al.*, "Deep structural analysis of novel B GaN material layers grown by MOVPE," *Journal of Crystal Growth*, vol. 315, no. 1, pp. 288–291, Jan. 2011, doi: 10.1016/j.jcrysgro.2010.08.042.
- [20] G. Orsal *et al.*, "Effect of boron incorporation on growth behavior of B GaN/GaN by MOVPE," *Journal of Crystal Growth*, vol. 310, no. 23, pp. 5058–5062, Nov. 2008, doi: 10.1016/j.jcrysgro.2008.08.024.
- [21] A. Said, M. Debbichi, and M. Said, "Theoretical study of electronic and optical properties of BN, GaN and BxGa1-xN in zinc blende and wurtzite structures," *Optik*, vol. 127, no. 20, pp. 9212–9221, Oct. 2016, doi: 10.1016/j.ijleo.2016.06.103.
- [22] A. Ougazzaden *et al.*, "Bandgap bowing in B GaN thin films," *Applied Physics Letters*, vol. 93, no. 8, Aug. 2008, doi: 10.1063/1.2977588.
- [23] T.-C. Han, H.-D. Zhao, and X.-C. Peng, "Short-gate AlGaIn/GaN high-electron mobility transistors with B GaN buffer," *Chinese Physics B*, vol. 28, no. 4, Apr. 2019, doi: 10.1088/1674-1056/28/4/047302.
- [24] Siegfried Selberherr, *Analysis and simulation of semiconductor devices*. 1984.
- [25] N. Nepal, J. Li, M. L. Nakarmi, J. Y. Lin, and H. X. Jiang, "Temperature and compositional dependence of the energy band gap of AlGaIn alloys," *Applied Physics Letters*, vol. 87, no. 24, Dec. 2005, doi: 10.1063/1.2142333.
- [26] Michael E. Levinshtein, Sergey L. Rumyantsev, and Michael S. Shur, *Properties of advanced semiconductor materials GaN, AlN, InN, BN, SiC, SiGe*, Wiley. New York, 2001.
- [27] Joachim Piprek, *Semiconductor optoelectronic devices: introduction to physics and simulation*. Academic Press; 1st edition, 2003.
- [28] O. Ambacher *et al.*, "Two dimensional electron gases induced by spontaneous and piezoelectric polarization in undoped and doped AlGaIn/GaN heterostructures," *Journal of Applied Physics*, vol. 87, no. 1, pp. 334–344, Jan. 2000, doi: 10.1063/1.371866.
- [29] I. Vurgaftman, J. R. Meyer, and L. R. Ram-Mohan, "Band parameters for III-V compound semiconductors and their alloys," *Journal of Applied Physics*, vol. 89, no. 11, pp. 5815–5875, Jun. 2001, doi: 10.1063/1.1368156.
- [30] D. M. Caughey and R. E. Thomas, "Carrier mobilities in silicon empirically related to doping and field," *Proceedings of the IEEE*, vol. 55, no. 12, pp. 2192–2193, 1967, doi: 10.1109/PROC.1967.6123.
- [31] SILVACO, *Atlas user's manual device simulation software*. 2010.
- [32] M. Gassoumi, A. Helali, H. Maaref, and M. Gassoumi, "DC and RF characteristics optimization of AlGaIn/GaN/B GaN/GaN/Si HEMT for microwave-power and high temperature application," *Results in Physics*, vol. 12, pp. 302–306, Mar. 2019, doi: 10.1016/j.rinp.2018.11.063.
- [33] Y. Zhang *et al.*, "High-performance AlGaIn double channel HEMTs with improved drain current density and High breakdown voltage," *Nanoscale Research Letters*, vol. 15, no. 1, Dec. 2020, doi: 10.1186/s11671-020-03345-6.
- [34] D. A. Deen, D. F. Storm, D. Scott Katzer, R. Bass, and D. J. Meyer, "Suppression of surface-originated gate lag by a dual-channel AlN/GaN high electron mobility transistor architecture," *Applied Physics Letters*, vol. 109, no. 6, Aug. 2016, doi: 10.1063/1.4961009.

BIOGRAPHIES OF AUTHOR



Hamida Djelti    received the Ph.D. degree in telecommunication from Aboubekr Belkaid University of Tlemcen, Algeria in 2013. She is currently Lecturer at the Department of Telecommunication, University of Tlemcen. She is a member of STIC laboratory in the same University. Her current research interests include the modeling and simulation of the semiconductor devices such as the Mosfet's and III-N (GaN, AlGaIn, B GaN, and InGa) high electron mobility transistor (HEMT). She can be contacted at email: hamida.djelti@univ-tlemcen.dz.